Experimental Investigation of the Far Field on OMEGA with an Annular Apertured Near Field

Uyen Tran

Advisor: Sean P. Regan

Laboratory for Laser Energetics Summer High School Research Program 2001

Abstract

Far field intensity distributions of an OMEGA laser beam were measured with either an annular or a circular aperture placed in the near field. Annular and circular apertures were constructed and installed in the down-collimated beam of the OMEGA Wavefront Sensor (OWS). The annular aperture blocked the central portion of the beam with radii less than two thirds of the near field radius, while the circular aperture allowed only the central portion of the beam to propagate to the far field. One-nanosecond square laser pulses smoothed with 1 THz Smoothing by Spectral Dispersion (SSD) and polarization smoothing were studied. Power spectra of far fields measured with the UV Equivalent Target Place (UVETP) diagnostic were computed for each aperture and compared with measurements of the standard configuration on OMEGA with no near field aperture. Simulations show good agreement with the experimental data.

Introduction

Laser beam smoothing is essential for direct-drive inertial confinement fusion. Nonuniformities in laser irradiation imprint target mass perturbations, which seed the ablative Rayleigh-Taylor hydrodynamic instability and degrade target performance. Single beam laser-irradiation nonuniformities are reduced using the following smoothing techniques: (1) smoothing by spectral dispersion (SSD), (2) distributed phase plates (DPPs), and (3) polarization smoothing (PS).

This investigation centered mainly upon the measurements of far field intensity distributions of an OMEGA laser beam with an annular apertured near field, a circular near field and a non-apertured near field. The non-apertured near field is the standard configuration used on OMEGA and is the control in this experiment. The apertures were constructed and installed in the down-collimated beam of the OMEGA Wavefront Sensor (OWS). One aperture was a circle with a diameter of two-thirds the diameter of the OMEGA near field and the other aperture, an annulus, was the inverse of the circular aperture. Far fields of one-nanosecond square laser pulses smoothed with 1 THz SSD and polarization smoothing (PS) were recorded with the ultraviolet equivalent target plane (UVETP) diagnostic and power spectra were calculated. Simulations are shown to be in good agreement with the experimental results.

The following sections discuss (1) the simulations of the near field, the far field, and the power spectral density of the far field intensity distribution and what they signify, (2) the construction and installation of near field apertures on the OWS and the far-field measurements with the ultraviolet equivalent target plane (UVETP) diagnostic, and (3)

the results of this investigation. The discussed results can be extrapolated to SSD smoothing of beams that irradiate only a portion of the phase plate, such as the dynamic focal spot size using a static phase plate.

Far Field Analysis

Using computer codes written in the PV-WAVE language, models were made to simulate the near field of the OMEGA laser beam. The first type of near field that was modeled was the near field that corresponds to the control in this experiment. This is a near field without an aperture. The diameter of the circular near field on OMEGA is approximately 27 cm as seen in Fig. 1a. The modulus squared of the two-dimensional Fourier transform of the UV near field electric field is the far field, which is shown in Fig. 1b. Taking another Fourier transform yielded an image shown in Fig. 1c that resembled the near field. But more importantly, this image allowed the power spectrum of the far field intensity distributions to be analyzed. To obtain the power spectrum, the azimuthal sum of the square of the Fourier amplitudes was taken. The power spectrum is the intensity of the beam at various wave numbers k. The power spectral density (PSD) in Fig. 1d can be used to quantify the smoothness of the laser beam intensity profile. For example, one may compare the PSD of one model to another, or one experiment to another, or even a model to an experiment. Smoothing can also be compared by calculating the single beam irradiation nonuniformity σ_{rms}, which is defined as the square root of the ratio of the power in the high frequencies ($k>0.04\ \mu m^{-1}$) to the power in the low frequencies ($k<0.04\ \mu m^{-1}$). The σ_{rms} of the beam modeled in Fig.1 without SSD and PS is 100%. Laser beam smoothing reduces the σ_{rms}.

Secondly, a model of a near field with a circular aperture in place was created using PV-WAVE. The circular aperture made the near field a circle with a diameter of approximately 18 cm, or two thirds of the diameter of the non-apertured near field. This may be viewed in Fig. 2a. A far field image was obtained, shown in Fig. 2b, and it was noted that the speckle pattern produced contained speckles that were larger than those of the far field produced by a Fourier transform of a near field without an aperture. The power spectrum for the far field produced by this type of near field was calculated (Fig. 2c) and analyzed. The power spectrum shown in Fig. 2d resembled the one produced by the non-apertured near field, but a notable difference was that this graph, Fig. 2d, had a lower cutoff wavenumber than the graph associated with the near field without an aperture. This can be explained when one compares Fig. 1c with Fig. 2c. Both of the images are circular, but Fig 1c has more power at larger radii. The equation used to calculate the cut-off wave number is given as $2\pi D/\lambda F$ where D=27 cm is the diameter of the OMEGA beam, λ=0.351 μm is the laser wavelength, and F=180 cm is the focal length of the OMEGA lens. When the circular aperture was placed in the near field, it caused the near field to have a smaller diameter. Nothing was changed in this equation except for D, which is directly proportional to k. Therefore if D gets smaller so does k.

A third near field with an annular aperture was modeled. This aperture made the near field a ring with a maximum diameter of 27 cm and a minimum diameter of 18 cm as shown in Fig. 3a. The far field here was also calculated. The result is in Fig. 3b. It was observed that the speckles produced were notably smaller than those of the far field created by the control. So the trend thus far is that the larger the near field the smaller the

speckle in the far field. Next, the power spectrum of this far field was obtained. The power spectrum is shown in Fig. 3d. It was compared to that of the non apertured near field in Fig. 1d and it was found that the graph of the PSD for the annulus had a different shape than that of the non-apertured near field, but the cutoff wavenumber was the same. Figures 1, 2, and 3 show how the near field irradiance affects the power spectrum of the far field intensity distributions.

Near Field Apertures

Before any data could be taken, the apertures had to be fabricated and installed in the near field. The beam used in this experiment was down-collimated with the OWS to 63 mm which is equivalent to 30 cm in the OMEGA near field and allows for the use of smaller apertures and easy modification of the near field. The circular aperture was fabricated to allow only a small amount of the beam in the shape of a 1.637 in. diameter circle to pass from the near field to the far field. The annular aperture was made in the same way but in lieu of a circle, a ring with an outer diameter of 2.48 in. and an inner diameter of 1.637 in. blocked the central portion of the beam and allowed the outer portion of the beam to pass from the near field to the far field. The diameter of the circular aperture and the inner diameter of the annulus are equivalent to the two-thirds the diameter of the near field on OMEGA. These apertures are shown in Fig. 4. They were fabricated in the LLE machine shop.

Installation of the near field apertures on the OWS required more hardware to be made. The translator that the apertures were to be mounted on couldn't hold the apertures as they were. Rods and brackets were fabricated to allow the apertures to be compatible

with the translator, and to place the apertures at the height of the beamline of the OWS. This height was approximately 10 in. The rods were able to move vertically which allowed for precision alignment in that direction. The brackets had to allow the desired amount and shape of the beam to pass, which was kept in mind as the brackets were designed. As shown in Fig. 4, the bracket for the circular aperture was made with two tapped holes to fasten the aperture to the bracket and one through hole to connect the bracket to the rod. The bracket for the annular aperture was made in a similar fashion; however, it had to have a cut out between the two tapped holes (see Fig. 4). This was because without the cut out, a part of the beam would have been obstructed. An obstruction such as the one that would have been produced by the bracket would have been unfavorable due to the fact that it would have altered the near field in a way that was unwanted.

Experimental Results

The investigation was conducted on the OWS. This is where 4% of the energy from an OMEGA beam is delivered for sampling. In this investigation, the beam propagates through a distributed phase plate (DPP) and an OMEGA lens. Next, the beam is down-collimated to a diameter of approximately 6 cm. The near field aperture positioned in the down-collimated beam of the OWS is shown in Fig. 5.

The aperture was mounted on a translator and then aligned to the center of the beam on the OWS. Steps were taken to record the exact positions that would allow the apertures to be centered properly. The rods had mechanical locks that kept the height properly aligned with the optic axis of the OWS, and the translator was marked to record

the horizontal location that would keep the aperture aligned to the center of the beam. During an OMEGA laser shot the far field of one of the apertures was recorded on a charged coupled device (CCD) of the UVETP diagnostic. When the data acquisition was completed, the aperture that was in the near field was replaced with another one and the procedure was again performed.

The Fourier transforms of the far fields were calculated using PV-WAVE and the PSD's of each of the near field apertured beams were compared to their respective models. Laser beam smoothing simulations of the 1 ns square laser pulse smoothed with 1 THz SSD and PS were performed by Dr. John Marozas for the three apertured near fields. Laser beam smoothing was not simulated in the models presented in figures 1-3. The laser beam smoothing effects of 1 THz SSD and PS are obvious after viewing the simulated power spectra shown in Fig. 6. Fig. 6a shows the power spectrum of the far field with an annular near field aperture and no laser beam smoothing, and Fig. 6b shows the power spectrum of the far field with an annular aperture and 1 THz SSD and PS. Simulations to account for 1 THz SSD and PS were run on the far fields that were recorded on OMEGA for the three apertures and the power spectra of the far field intensity distributions were calculated. The SSD smoothing technique involved temporal integration. The power spectra recorded for each aperture at the initial time looked similar to those presented in figures 1-3, except they had a lower σ_{rms} because of the PS. The power spectra of the time integrated far fields simulated with 1 THz SSD and PS were found to be in good agreement with the experimental data for all the near field apertures that were studied. Fig. 7 contains the results for the annular near field aperture.

The power spectrum at the beginning of the laser pulse is also shown for reference. Notice how it (thin curve) has higher intensity modulations than the curves with the laser beam smoothing of 1 THz SSD and PS. The simulation (the thicker solid line) is plotted over the measured power spectrum (the dotted line) and they appear to be in good agreement. Fig. 8 has the results for the circular near field aperture. Once again the thin black line is the power spectrum without SSD, and the simulated data shows good agreement with the measured results. Fig. 9 shows the simulated and experimental power spectra for the standard configuration on OMEGA. Again, the thin curve is the model without SSD and the thicker line is the model with smoothing which shows good agreement with the measured power spectrum (the dotted line). The general shapes of the lines in Fig. 8 look similar to these, but the cut-off wave number for Fig. 8 is less. The cut-off wave number for Fig. 7 is the same as this one, but the shapes of the power spectra differ because of the different near field aperture shapes.

Conclusion

Far field intensity distributions of an OMEGA laser beam were measured with either an annular or a circular aperture placed in the near field. Models were created with PV-WAVE to understand the relationship between the near field irradiance and the power spectrum of the far field intensity distributions. Hardware was fabricated to install annular and circular apertures in the down-collimated beam of the OWS. One-nanosecond square laser pulses smoothed with 1 THz SSD and polarization smoothing were studied. Power spectra of far fields measured with the UVETP diagnostic were computed for each aperture and compared with measurements of the standard

configuration on OMEGA with no near field aperture. Laser beam smoothing simulations show good agreement with the experimental data. Results from this investigation can be extrapolated to SSD smoothing of beams that irradiate only a portion of the phase plate, such as the dynamic focal spot size using a static phase plate.

Acknowledgments

Thank you to Dr. Craxton for allowing me to participate in this program. Few high school students have the opportunity to work with the OMEGA laser system or the scientists who work on OMEGA. I am truly fortunate. Thank you also to Dr. Marozas for the simulations. Without the simulations, I would have nothing to compare the experimental data with. I give special thanks to my advisor Dr. Regan. He was patient with me when explaining concepts and helped me to complete this study. He taught me how scientists conduct experiments each step of the way. Thank you.

Figure Captions

Figure 1. The models for the standard configuration used on OMEGA created using PV-Wave are shown here. The near field intensity is shown in (a), the modulus squared of the 2-D Fourier transform of the UV near field electric field is the far field shown in (b) and the Fourier transform of (b) is used to evaluate the power spectrum in (c), notice how it resembles the near field. Power spectral density is shown in (d) which is the azimuthal sum of the square of the Fourier amplitudes.

Figure 2. These are models for the circular aperture. The image (a) is the near field intensity, (b) is the far field intensity, notice how the speckles are larger here than for Fig. 1b. (c) is the Fourier transform of (b) and (d) is the power spectrum. Notice that the cut-off wave number for this power spectrum is less than the one for Fig. 1d. This is because the diameter of the circular near field is smaller, so the cut-off wave number has to be smaller.

Figure 3. These are models for the annular aperture. The image (a) is the near field intensity, which now looks like a ring because the aperture is blocking the central portion. (b) is the far field intensity, notice that speckles are smaller here than for Fig. 1b. (c) is the Fourier transform of the (b) and (d) is the power spectrum. The cut-off wave number is the same as in Fig. 1d because the diameters are the same, but the shape is different due to the annular near field aperture.

Figure 4. These are the near field apertures. The diameter of the circle and the inner diameter of the annulus are equal to 1.637 in. The apertures can be this small when the beam is 30 cm because the beam was down-collimated to 63 mm on the OWS. So the diameter of the apertures above is really just a little less than two-thirds of the near field diameter on OMEGA.

Figure 5. This is the experimental setup. The table is the OWS in the OMEGA target bay. A sample beam with 4% of the laser light energy is passed through a DPP and an OMEGA lens. The beam is then down-collimated, passed through an aperture, and brought to a focus on a CCD camera to measure the far field.

Figure 6. These are power spectra for the annulus. The graph of (a) is the one modeled with PV-Wave. It didn't take into account SSD so the σrms was high. Graph (b) is the power spectrum of the far field of a 1 ns square laser pulse smoothed with 1 THz SSD and PS, so the intensity modulations were much lower.

Figure 7. This graph shows the power spectra for the annulus. Notice how the thin curve has a higher intensity than the curves with the laser beam smoothing of 1 THz SSD and PS. The simulation (the thicker solid line) is plotted over the measured power spectrum (the dotted line) and they appear to be in good agreement.

Figure 8. The power spectra for the circular aperture are shown here. Once again the

thin black line is the power spectrum without SSD. The dotted line is the measured spectrum with 1 THz SSD and PS. The thicker solid curve represents the simulated data with 1 THz SSD and PS and shows good agreement with the experimental result.

Figure 9. These are the power spectra for the standard configuration on OMEGA. Again, the thin curve is the model without SSD and the thicker line is the model with smoothing which shows good agreement with the measured power spectra (the dotted line). The general curve of the lines in Fig. 8 look similar to these, but the cut-off wave number for Fig. 8 is less. The cut-off wave number for Fig. 7 is the same as this one, but the shapes differ.

Fig.1

(a)

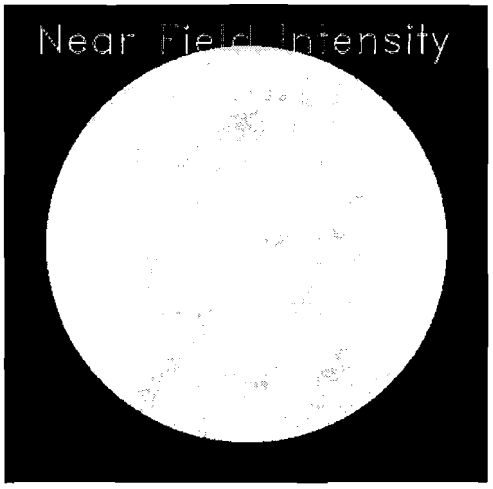
Near Field Intensity

(b)


Far Field Intensity
cir

(c)

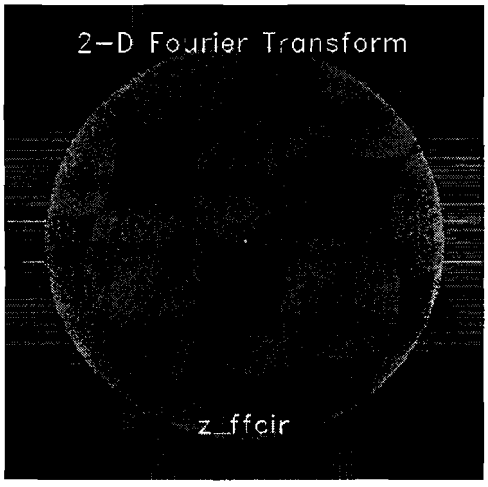
2-D Fourier Transform
z_ffcir

(d)

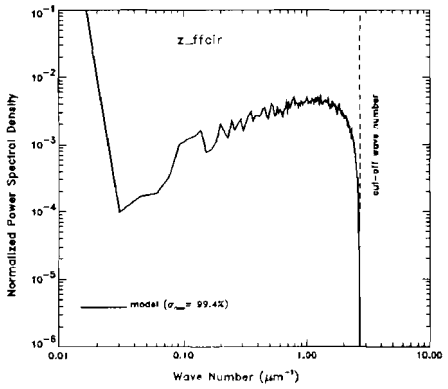
z_ffcir
Normalized Power Spectral Density
cut-off wave number
model (σ_rms = 99.4%)
0.01
0.10
1.00
10.00
Wave Number (μm⁻¹)

Fig. 2

(a)


Near Field Intensity
scir

(b)

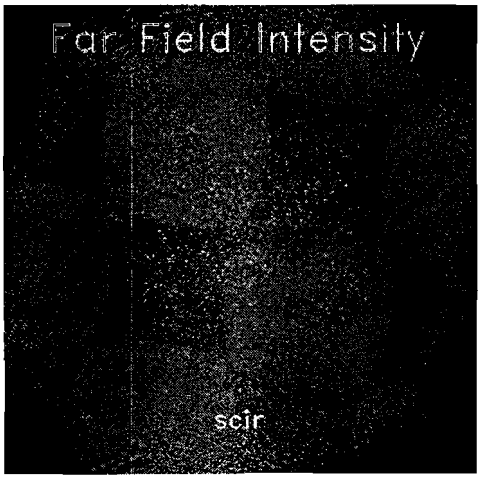
Far Field Intensity
scir

(c)


2-D Fourier Transform
z_ffscir

(d)

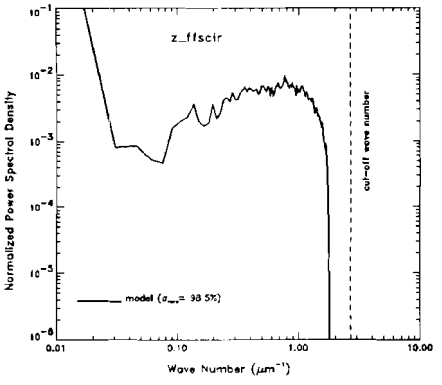
z_ffscir
Normalized Power Spectral Density
cut-off wave number
model
0.01
0.10
1.00
10.00
Wave Number

Fig. 3

(a)

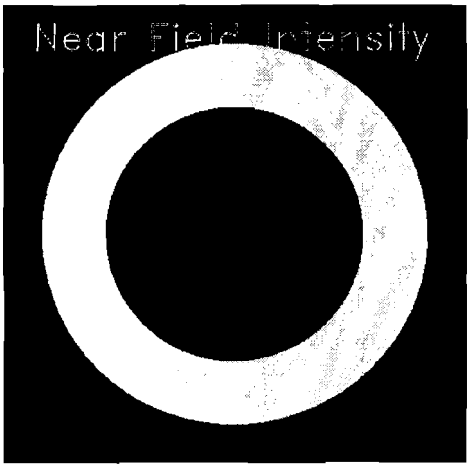
Near Field Intensity

(b)

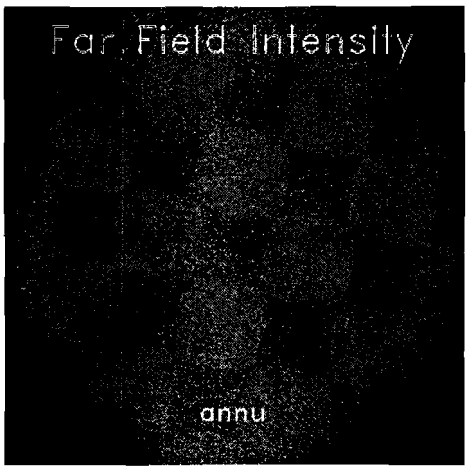
Far Field Intensity
annu

(c)

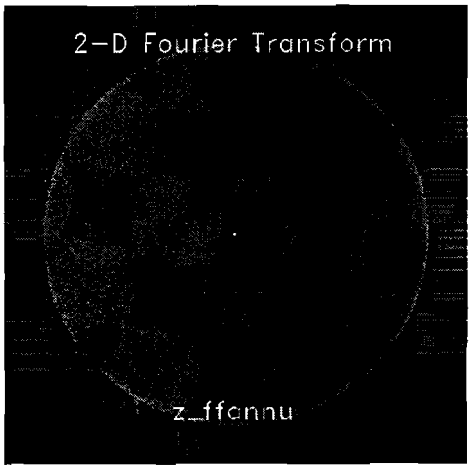
2-D Fourier Transform
z_ffannu

(d)

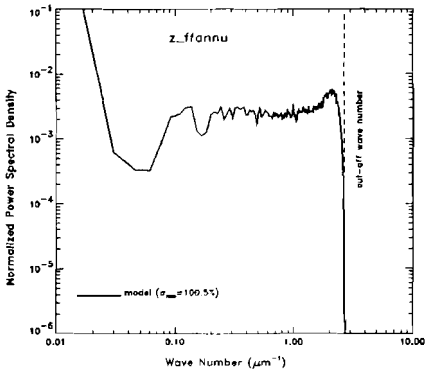
z_ffannu
Normalized Power Spectral Density
cut-off wave number
Wave Number (μm⁻¹)
0.01
0.10
1.00
10.00

Fig. 4

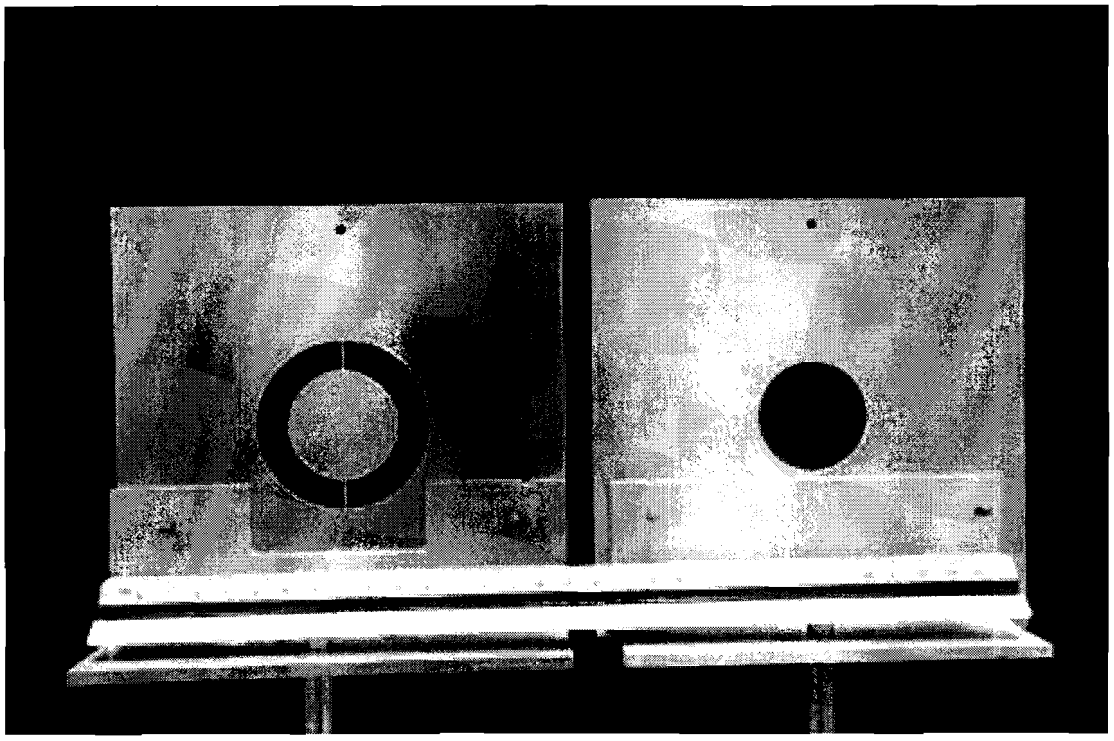

Fig. 5

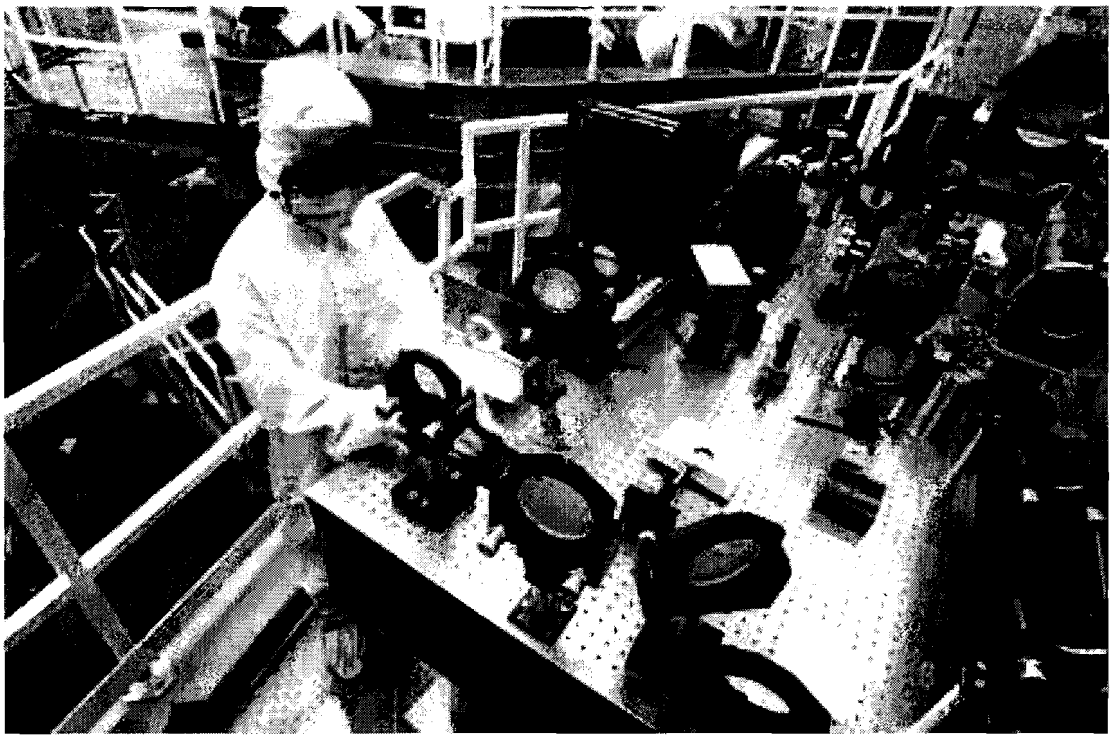

Fig. 6

(a)

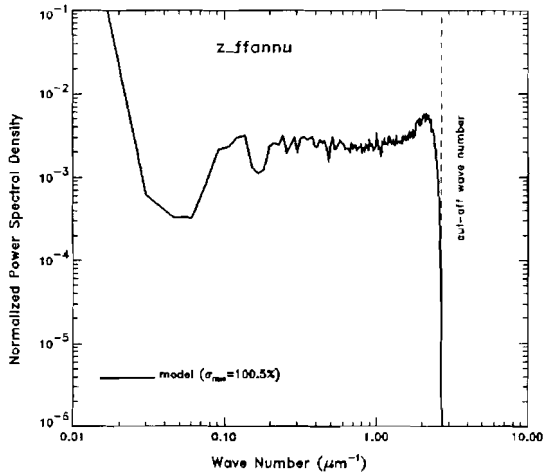
z_ffannu
Normalized Power Spectral Density
Wave Number (μm^{-1})
cut-off wave number
model (σ_{rms}=100.5%)
10^{-1}
10^{-2}
10^{-3}
10^{-4}
10^{-5}
10^{-6}
0.01
0.10
1.00
10.00

(b)

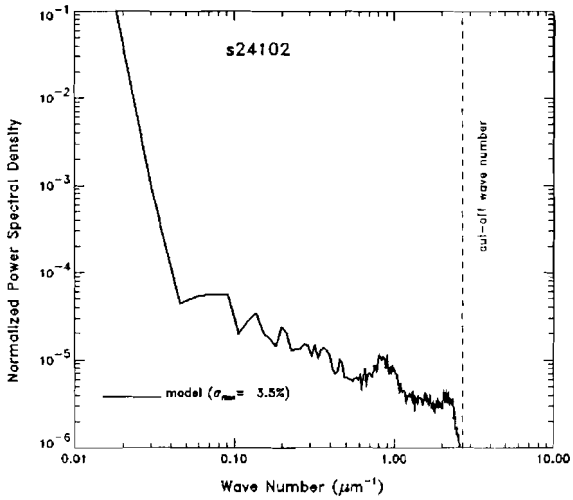
s24102
Normalized Power Spectral Density
Wave Number (μm^{-1})
cut-off wave number
model (σ_{rms}= 3.5%)
10^{-1}
10^{-2}
10^{-3}
10^{-4}
10^{-5}
10^{-6}
0.01
0.10
1.00
10.00

Fig. 7

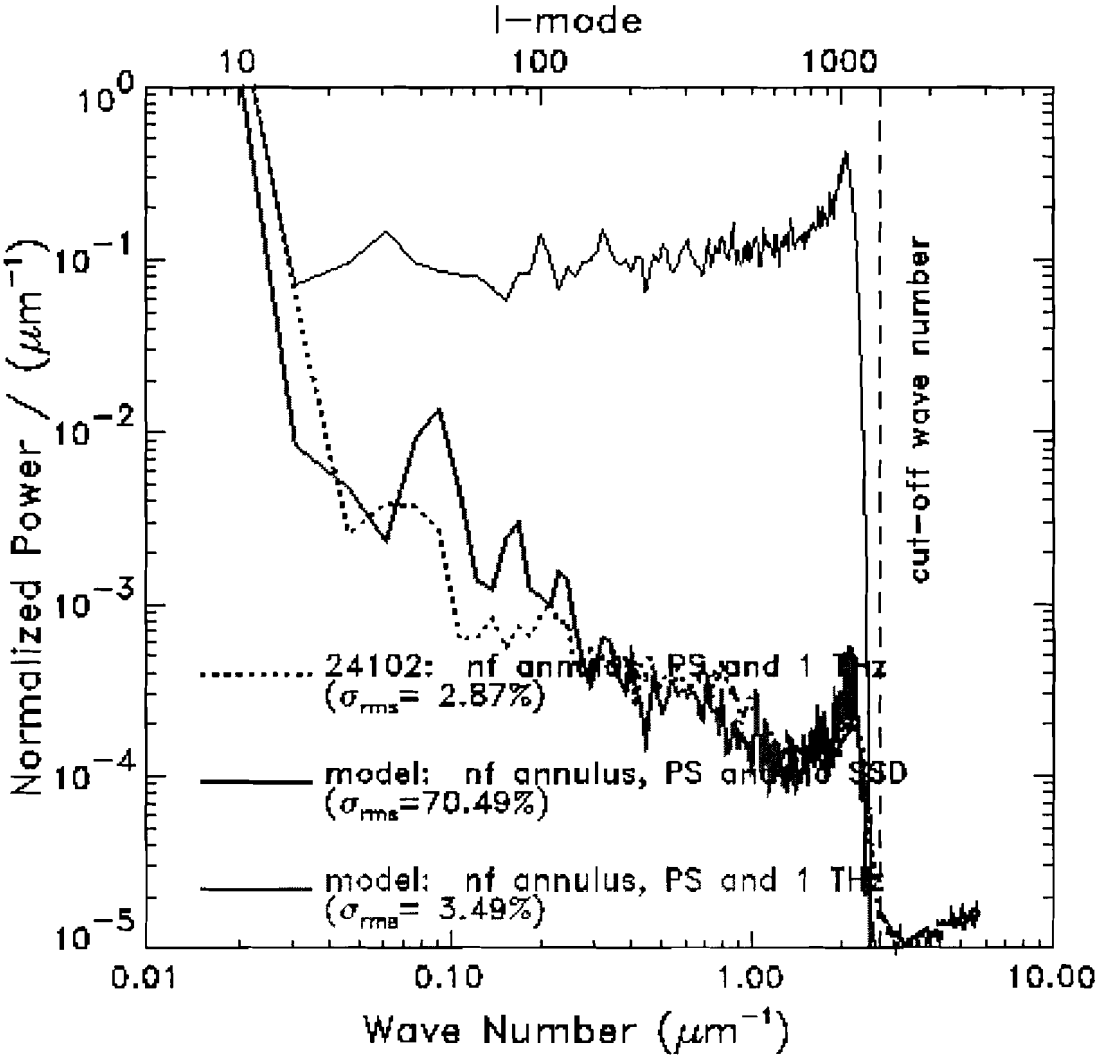
l−mode
10
100
1000
10^0
10^{-1}
10^{-2}
10^{-3}
10^{-4}
10^{-5}
Normalized Power / (μm^{-1})
cut−off wave number
24102: nf annulus, PS and 1 THz
(σ_{rms}= 2.87%)
model: nf annulus, PS and no SSD
(σ_{rms}=70.49%)
model: nf annulus, PS and 1 THz
(σ_{rms}= 3.49%)
0.01
0.10
1.00
10.00
Wave Number (μm^{-1})

Fig. 8

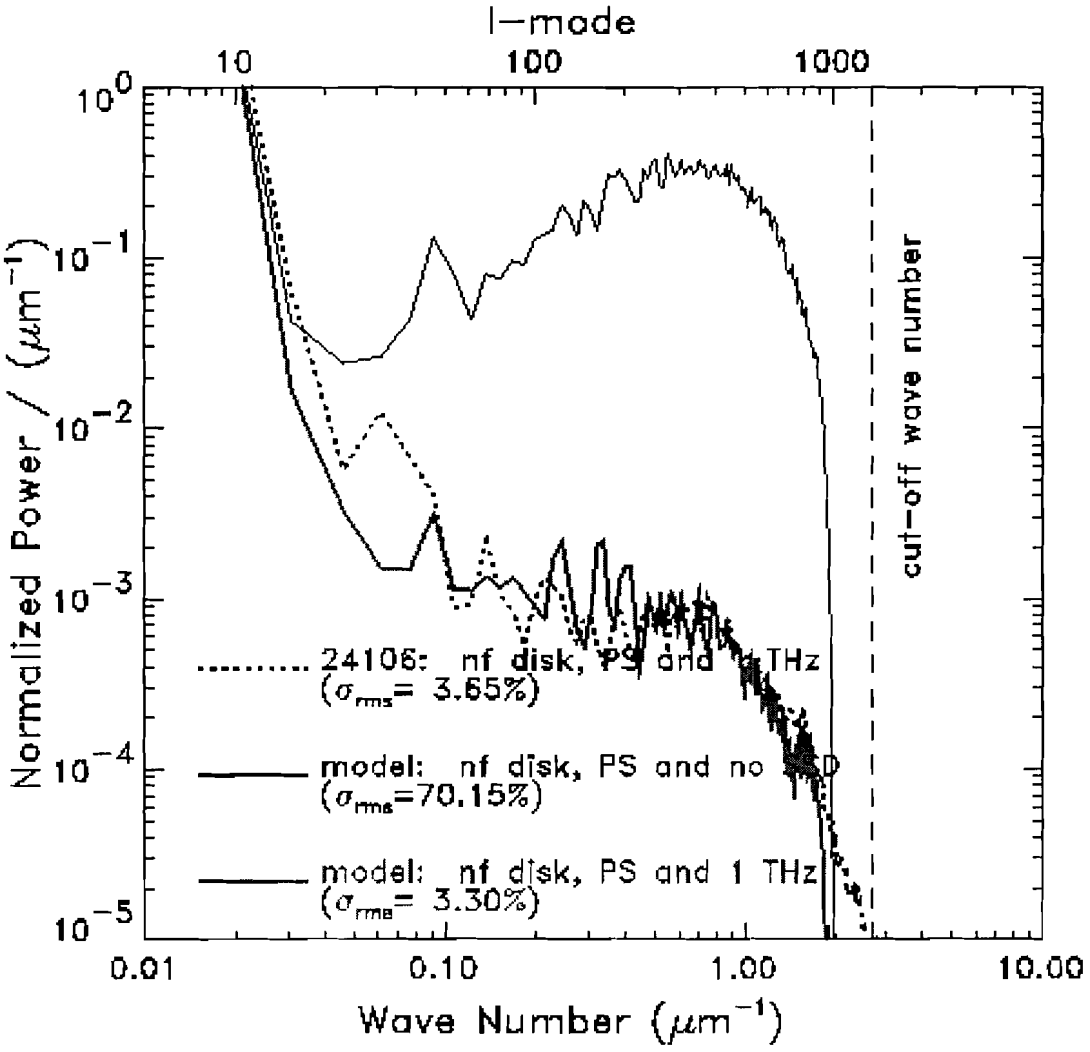
l−mode
10
100
1000
10^0
10^{-1}
10^{-2}
10^{-3}
10^{-4}
10^{-5}
Normalized Power / (μm^{-1})
cut−off wave number
24106: nf disk, PS and 1 THz
(σ_{rms}= 3.65%)
model: nf disk, PS and no THz
(σ_{rms}=70.15%)
model: nf disk, PS and 1 THz
(σ_{rms}= 3.30%)
0.01
0.10
1.00
10.00
Wave Number (μm^{-1})

Fig. 9

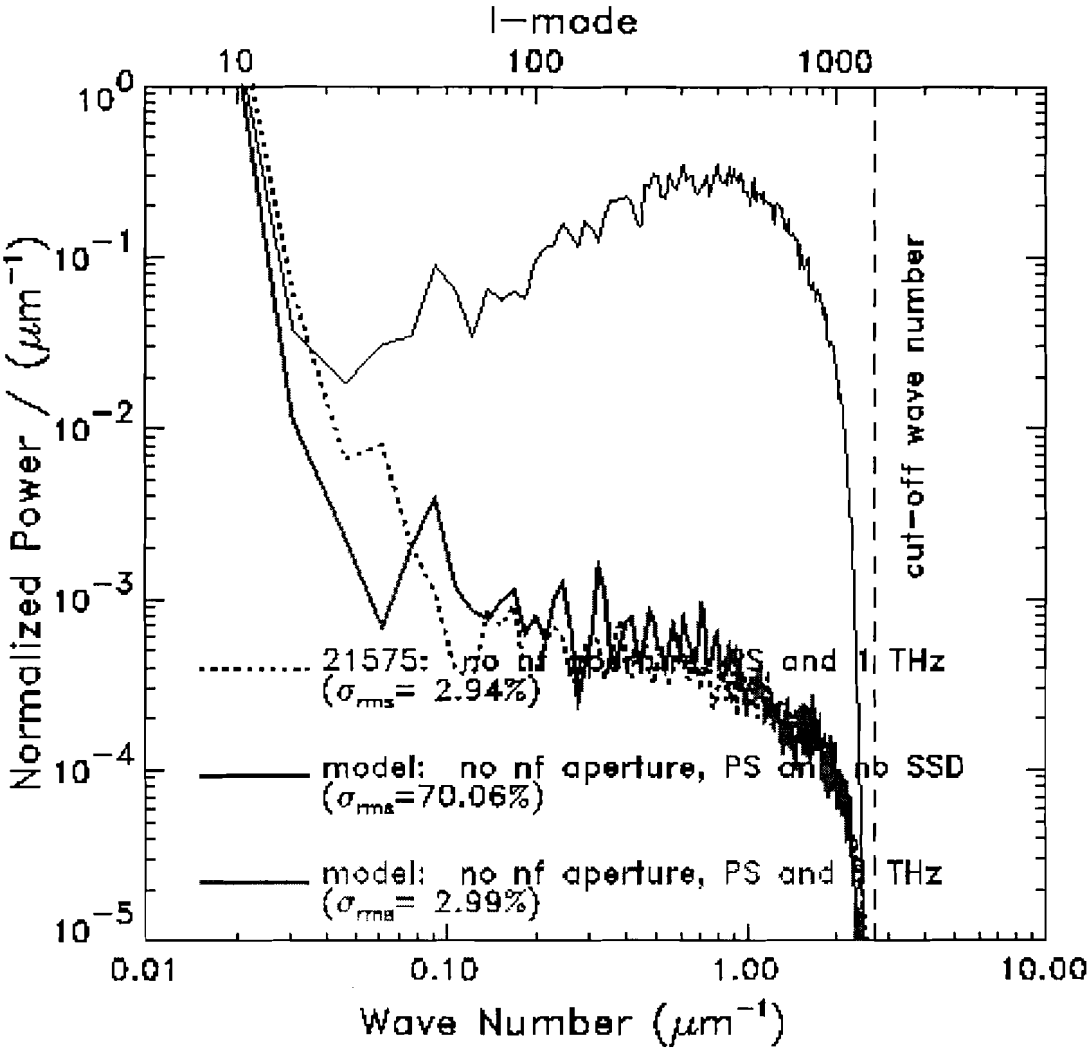
l−mode
10
100
1000
10^0
10^{-1}
10^{-2}
10^{-3}
10^{-4}
10^{-5}
Normalized Power / (μm^{-1})
cut−off wave number
21575: no nf aperture, PS and 1 THz
(σ_{rms}= 2.94%)
model: no nf aperture, PS and nb SSD
(σ_{rms}=70.06%)
model: no nf aperture, PS and 1 THz
(σ_{rms}= 2.99%)
0.01
0.10
1.00
10.00
Wave Number (μm^{-1})